

SoftSense: Collaborative Surface-based Object Sensing and Tracking Using Networked Coils

Kai Li, Ufuk Muncuk, M. Yousof Naderi, Kaushik R. Chowdhury
Dept. of Electrical and Computer Engineering Northeastern University, Boston, MA, USA
{likai2,umuncuk}@coe.neu.edu, {naderi,krc}@ece.neu.edu

Abstract—Object sensing and tracking using electric and magnetic fields allow intelligent interaction, automation, and adaptation in cyber-physical systems. Our approach, called Softsense, uses a software-defined collaborative sensing technique for detection of the type of object and where it is placed on a large surface. Unlike RF based sensing approaches that are generally dependent on channel conditions, capacitive sensing that detects only low conductive objects, and Qi-based inductive sensing that is effective at few mm in range, Softsense is designed to operate without the above limitations. Softsense is cost effective, low power and scalable, which allows extension over large surfaces. First, we introduce a dual-coil inductive sensing architecture based on nested coils, i.e., passive (outer) and active (inner) coils, for low-power contact-less sensing. A data driven support vector machine-based approach helps to classify different materials using the voltage readings obtained at the passive coil. SoftSense combines sensed voltage information from multiple different coils spread over the surface for collaborative sensing. We validate our design on a real sensing prototype with customized coils, fabricated sensing circuit, and a network software controller. Experimental results show that each sensing coil only consumes few milliwatts, i.e., 18x less than the inductive sensing and 15x less than classical magnetic resonance sensing, extends sensing depth to 3 cm, and enables coverage of large surface sensing.

Index Terms—contactless sensing, magnetic resonance, object detection and tracking

I. INTRODUCTION

Object detection and tracking based on both far and near electromagnetic fields have been studied extensively over the past several years. While great strides have been made, existing solutions have several limitations: Radio frequency (RF) based far-field sensing solutions require specialized circuits and antenna design, with the risk of consuming high power at the transmitter. Though RF energy harvesting [1] can be used in short-range sensing for wake-up radios, other wireless localization solutions based on reflected RF signals from Bluetooth, Zigbee, RFID [2], Wi-Fi, UWB radios [3], backscatter [4] require a second (receiver) device and/or additional signal reflectors to send feedback to transmitter side to estimate the channel state. State of the art near-field magnetic induction based sensing solutions, such as the analog and digital sensing in Qi [5], are limited in distance to few mm, but also requires perfect alignment between the sensing coil and the object. Industry standard Qi solutions today allow one object sensing per coil and incur a power cost of $\frac{1}{3}$ W per coil, which makes it costly and complex to scale over a large area. Finally, other low-cost sensing solutions such as resistive sensing [6] and

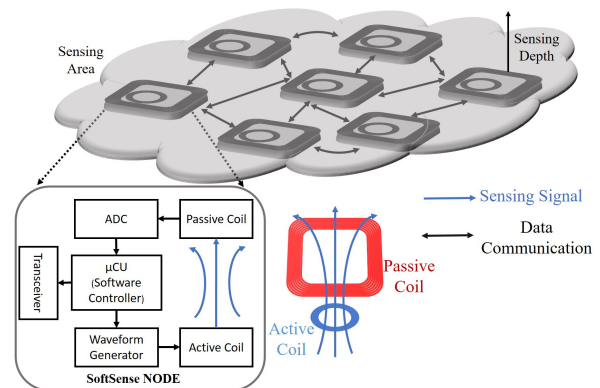


Fig. 1: System overview of SoftSense nodes and network with low-power distributed sensing over surface and distance.

capacitive coupling [7] are not capable of sensing materials other than low-conductive objects.

This paper proposes SoftSense, the first-of-its-kind multi-coil sensing network to detect and track various objects in real time. Our approach is agnostic of the object shape and enables a low-power, over-distance, and large area sensing solution. We note that this is achieved without any need of: (i) modification to the object that is being sensed, (ii) complex channel estimation, and (iii) continuous feedback from the receiver.

• **SoftSense Operational Overview:** Fig. 1 depicts an overview of our system architecture and components. Each node consists of an active coil, a passive coil, a sensing circuit, transceiver, and a software controller. The inner, smaller coil is connected to the continuous wave generator, and the outer, bigger coil acts a passive coil. The coils are so designed such that they are in resonance with each other, when there is active current in the smaller coil and no object is placed on the surface. Thus, the passive coil acts a resonator relay that extends the magnetic flux generated by the current with extremely low power consumption. Each such dual-coil sensing element (henceforth called as a *node*) operates in the kHz band. The coils are networked together and exchange control messages with the network controller. Multiple *nodes* are attached to the underside of a large surface such as a desk, and as long as the separation width between the sensing object and the node array is less than 3cm, Softsense can operate with high accuracy. When an object is placed on the surface, each node

measures the induced voltage in the outer coil and reports back these measurements, along with its ID, to the central controller. Similarly, if the object moves, the nodes detect similar changes and transmit update messages to the controller. The central controller fuses all the measurement data reported by the entire node array and matches the voltage patterns with a priori stored signatures.

• **SoftSense Design Challenges:** Regardless of the design and sensing technology, the dimensions of the coils influence majorly the performance of sensing. For sensing with low-power consumption (in range of mW), both inductive and magnetic resonance-based approaches provide only mm-scale sensing distance. Additionally, to cover a large area, solutions such as increasing the size of the sensing coil, using 1-1 proportion of coils per charging location increase system cost and overall power consumption exponentially. Furthermore, measurements by a given coil can result in missed detection. For example, consider the two object placement scenarios below that excite the coil to similar extents: (i) an object with a size bigger than sensing coil, (ii) a larger object that covers multiple coils but with a partial coverage of each sensing coil, and a smaller object that covers part of only one sensing coil. Both situations give rise to similar voltage changes from the partially covered sensing coil. To address these challenges, we design a system that takes into consideration input data from multiple coils at the same time. Thus, there is a need for systematic measurements and algorithms to distinguish between voltage changes for different types of objects.

In summary, the SoftSense design incorporates the following hardware and software contributions:

- We design a dual-coil sensing architecture that enables low-power, contact-less sensing. It extends the effective sensing distance 5x times compared to current state-of-the-art coil sensing solutions such as Qi, and sensing coverage 4x times compare to single coil configuration at 18x energy savings.
- We conduct a set of experiments and demonstrate accurate detection of different objects over distance through software-based detection of voltage changes and object area coverage.
- We propose a multi-coil voltage gradient tracking method that can localize and track object motion over the surface.
- We build a prototype that consists of a sensing node with a software controller. We then deploy a node array under different surface materials to demonstrate real-time sensing over a large surface area.

The paper is organized as follows. In Section II, we review existing works related to wireless localization and tracking of objects. Section III discusses system design and theoretical analysis of the coils. Implementation aspects and experimental results are described in Section IV. Section V presents the conclusions and future works.

II. RELATED WORK

Localization and tracking solutions based on the reflected RF signals from technologies such as WiFi, Bluetooth, ZigBee,

LoRa, and RFID have been extensively studied [3], [8]. However, (i) multi-path reflections from the environment, (ii) need for a receiver device and/or additional signal reflectors, and (iii) complex and power consuming algorithms at the transmitter are the main shortcomings of these works. Recent advancements in smart-phones wireless charging have popularized coil-based object sensing, such as inductive-based backscatter [5]. However, coils need to be perfectly aligned and separated by less than 7 mm between receiver and transmitter. Magnetic MIMO [9], analogous to the concept of MIMO in RF signals, uses six power amplifiers to deliver power to a phone through a table. This uses current change from each coil as the feedback to localize the position of a given phone and then controls the current of each amplifier to beamform the power to the receiver. While the receiver does not need perfect alignment with the transmitter, each coil needs one amplifier, which drives up cost. Second, the current feedback induced from the mutual coupling between transmitter and receiver prolongs sensing time. Both the inductive coupling backscatter method and the magnetic resonant current sensing method need an additional coil inside the object, which limits the application of the sensing system. The contactless sensing system in SoftSense is motivated by the need to simplify sensing, increase the sensing distance and area, and provide flexibility as we do not need extra coils or circuits in the target object.

III. SYSTEM DESIGN AND THEORETICAL ANALYSIS

A. Magnetic dual-coil contact-less sensing

The concept of strongly coupled magnetic resonance used in SoftSense is based on coupled mode theory, which is utilized in wireless power transfer [10] to significantly extend the charging distance compared to the traditional 1:1 transmitter-receiver magnetic resonance or inductive charging.

Fig. 2a shows the circuits for strongly coupled magnetic resonance power transfer, where the source coil connects to the AC power source and generates the magnetic field. The oscillating magnetic flux resonates in the transmitter coil. On the other side, the magnetic flux from the transmitter is converted into the current in the receiver coil. This current creates a secondary magnetic flux within the load coil. This flux energy is converted into the current within the device represented as R_l . Fig. 2b shows the circuit schematic of our design and Fig. 2c shows its architecture with the two coils. Here, $d_{ol} = 12\text{ cm}$, $d_{il} = 10\text{ cm}$, $d_{od} = 5\text{ cm}$, $d_{id} = 3\text{ cm}$ are outer coil length, inner coil length, outer coil diameter, and inner coil diameter, respectively. Different from wireless power transfer, in the SoftSense magnetic contact-less sensing system, the objects do not have a receiver coil inside.

Various objects with relative high conductive materials such as cell phone, laptop, and mouse change the magnetic field distribution at the transmitter outer coil. This effect can be measured via voltage changes in the outer coil. The amount of change depends on multiple variables, such as size, shape, materials, magnetic permeability, electrical conductivity, and the overlapping area between object and the coil.

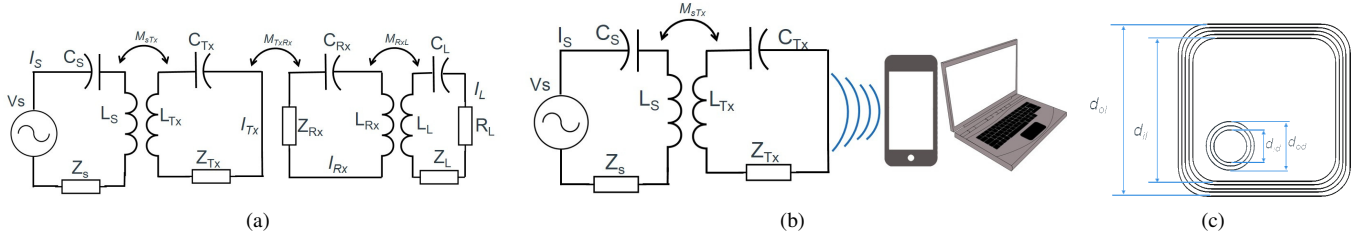


Fig. 2: Circuit schematics of (a) strongly coupled resonant wireless power transfer, (b) proposed dual-coil contact-less magnetic object sensing, and (c) dual-coil architecture with active inner and passive outer coils.

Next, we detail the theory behind strongly coupled resonant wireless transfer and accordingly introduce our object sensing analytical approach. Table (I) summarizes the circuit parameters used in our formulations. We assume the self-inductance, impedance, mutual inductance, resistance, and angular frequency of input AC signal are given, as they depend on characteristics of the hardware and coils. Then by using Kirchhoff's laws, we calculate the induced currents at the source, Tx, Rx, and load coils, shown in Fig. 2a.

TABLE I: Summary description symbols in circuit equations

Symbol	Description
V_s	Input AC signal voltage at source coil
I_s	Current amplitude at source coil
C_s	Capacitance at source coil
L_s	Self inductance at source coil
M_{sTx}	Mutual inductance between source and Tx
Z_s	Resistance of input AC signal at source coil circuit
I_{Tx}	Current amplitude at Tx coil
L_{Tx}	Self inductance at Tx coil
C_{Tx}	Capacitance at Tx coil
Z_{Tx}	Impedance of Tx circuit
M_{TxRx}	Mutual inductance between Tx and Rx
I_{Rx}	Current amplitude at Rx coil
L_{Rx}	Self inductance at Rx coil
C_{Rx}	Capacitance at Rx coil
Z_{Rx}	Impedance of Rx circuit
M_{RxL}	Mutual inductance between Rx and load
I_L	Current amplitude at load coil
L_L	Self inductance at load coil
C_L	Capacitance at load coil
R_L	Resistance of load coil
Z_{LTx}	Impedance of Tx coil
Z_{CTx}	Impedance of capacitor at Tx circuit
ω	Angular Frequency of AC source

$$V_s = I_s(j\omega L_s + \frac{1}{j\omega C_s} + Z_s) - j\omega M_{sTx} I_L \quad (1)$$

$$I_{Tx}(j\omega L_{Tx} + \frac{1}{j\omega C_{Tx}} + Z_{Tx}) + j\omega(M_{sTx} I_s - M_{TxRx} I_{Rx}) = 0 \quad (2)$$

$$I_{Rx}(j\omega L_{Rx} + \frac{1}{j\omega C_{Rx}} + Z_{Rx}) + j\omega(M_{RxL} I_L - M_{TxRx} I_{Tx}) = 0 \quad (3)$$

$$I_L(j\omega L_L + \frac{1}{j\omega C_L} + Z_L + R_L) + j\omega M_{34} I_s = 0 \quad (4)$$

In the case of magnetic dual-coil object sensing from Fig. 2b, both Rx and load coils are replaced by the object. Recall that the source coil is the smaller inner coil, and the

passive coil is the larger outer coil. Accordingly, the circuit equations for the dual-coil system can be explained by the following equations:

$$V_s = I_s(j\omega L_s + \frac{1}{j\omega C_s} + Z_s) - j\omega M_{sTx} I_{Tx} \quad (5)$$

$$I_{Tx}(j\omega L_{Tx} + \frac{1}{j\omega C_{Tx}} + Z_{Tx}) + j\omega M_{sTx} I_s = 0 \quad (6)$$

$$Z_{Tx} = Z_{LTx} + Z_{CTx} \quad (7)$$

Here, the change of current amplitude at the transmitter outer coil is negligible because the AC power of inner source coil is very low (mW). At resonant mode, $j\omega L_{Tx}$ and $j\omega C_{Tx}$ cancel each other. V_{Tx} is the voltage of outer coil when there is no object and can be calculated as follows:

$$V_{Tx} = j\omega M_{sTx} I_s \quad (8)$$

$$V_{Tx} = I_{Tx} Z_{Tx} = I_{Tx} (Z_{LTx} + Z_{CTx}) \quad (9)$$

Once an object comes within sensing coverage and distance, the impedance of the outer coil Z_{LTx} changes to Z'_{LTx} and accordingly the voltage change at the outer coil is calculated as:

$$|\Delta V| = |I_{Tx}(Z'_{LTx} - Z_{LTx})| \quad (10)$$

B. Multi-coil object detection, classification and tracking

In this section, we extend the SoftSense approach to object classification and tracking. While voltage readings in an individual coil can detect the presence of an object, they can not accurately predict the type of objects. Additionally, an individual coil is not capable of tracking an object over an area. For example, objects with different sizes and types but the same overlapping coverage with a sensing node can cause similar extent of voltage changes. To address these challenges and enable object tracking, we take into consideration readings from multiple coils at the same time. Accordingly, we propose and build a network of coils with a software-controller and a method of collaborative sensing and tracking.

Fig. 3 shows the idea of a multi-coil network, where each square block is a SoftSense node. As we see, $m \times k$ nodes cover a large surface area.

Object detection: To detect the presence of an object, each node senses individually within its sensing coverage and

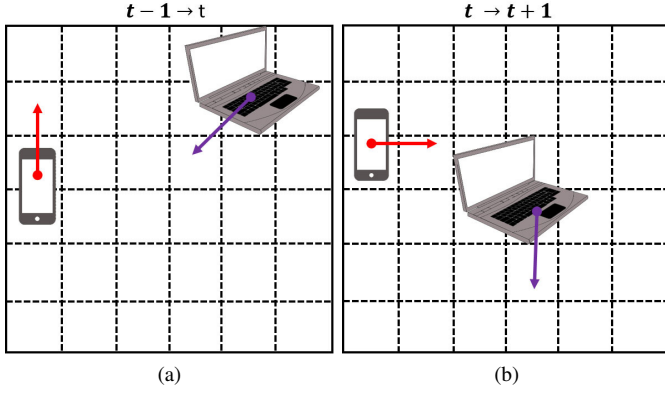


Fig. 3: Multi-coil network, where each square block denotes a sensing node. Objects transition around the surface (a) from time $t - 1$ to t , and (b) from t to $t + 1$.

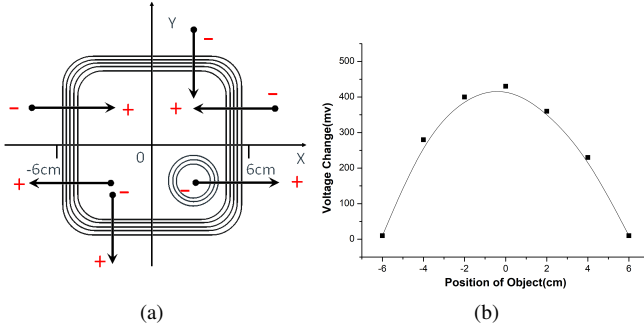


Fig. 4: Positive and negative voltage changes of a moving object (a) along the x and y axes of sensing coil, and (b) as function of distance from coil center.

shares voltage changes via the update messages to the central controller. In our current implementation, each SoftSense node senses at an interval of 20ms, and averages every 50 samples to get the latest sensed voltage. At time t , a *voltage matrix* of the sensing surface can be computed as follows:

$$V(t) = \begin{bmatrix} V_{11} & V_{12} & \dots & V_{1k} \\ V_{21} & V_{22} & \dots & V_{2k} \\ \vdots & \vdots & \ddots & \vdots \\ V_{m1} & V_{m2} & \dots & V_{mk} \end{bmatrix} \quad (11)$$

where V_{ij} denotes the sensed voltage of the node located at position (i, j) . Regardless of the type and size of the object, any sensed voltage higher than a given noise threshold (i.e. empirically determined based on experiments) indicates the presence of an object. Additionally, based on the voltage matrix, we can detect the presence of multiple objects over the surface and their positions, when V_{ij} is greater than the noise threshold.

Object classification: After object detection, we need to identify the type of each object, for which we leverage a Support Vector Machine (SVM) classifier. In particular, we divide our experimental data into a training and a testing set in a 4:1 ratio, i.e., for each object, out of five experiments, four are used for training and one is used for testing. Our feature vector consists of (i) range of possible sensed voltages, (ii)

number of covered nodes (i.e. connected blocks in Fig. 3). First, depending on the overlapping area between an object and sensing coil, the value of voltage change lies within a range as shown in Fig. 4. Accordingly, we collect sensing data for possible overlapping areas of an object and use the voltage range as our SVM feature. Second, it's possible that an object may cover one or more sensing nodes. We also consider this scenario and the numbers of coverable nodes by each object as an SVM feature in type classification.

Object tracking: Our collaborative tracking method first computes the voltage gradient matrix and then estimates the motion and direction of multiple moving objects through signs of ΔV elements in voltage gradient matrices. This voltage gradient matrix between time $t - 1$ and t is defined as:

$$\Delta V(t-1, t) = \begin{bmatrix} \Delta V_{11}^t & \dots & \Delta V_{1p}^t & \dots & \Delta V_{1j}^t & \Delta V_{1j+1}^t & \dots & \Delta V_{mk}^t \\ \vdots & \vdots \\ \Delta V_{i1}^t & \dots & \Delta V_{ip}^t & \dots & \Delta V_{ij}^t & \Delta V_{ij+1}^t & \dots & \Delta V_{ik}^t \\ \Delta V_{i+11}^t & \dots & \Delta V_{i+1p}^t & \dots & \Delta V_{i+1j}^t & \Delta V_{i+1j+1}^t & \dots & \Delta V_{i+1k}^t \\ \vdots & \vdots \\ \Delta V_{q1}^t & \dots & \Delta V_{qp}^t & \dots & \dots & \dots & \dots & \Delta V_{qk}^t \\ \vdots & \vdots \\ \Delta V_{m1}^t & \dots & \Delta V_{mp}^t & \dots & \Delta V_{mj}^t & \Delta V_{mj+1}^t & \dots & \Delta V_{mk}^t \end{bmatrix} \quad (12)$$

where ΔV_{ij}^t refers to change in voltage at the sensing coil located at position (i, j) , between time $t - 1$ and t . Furthermore, the negative and positive signs of ΔV_{ij}^t determine the direction of motion. As shown in Fig. 4, if an object is moving toward the center of sensing coil, the voltage changes are positive, and negative if it is moving away. This means the direction of motion is always from negative ΔV to positive. To demonstrate this, Fig. 3 shows two objects (i.e. phone and laptop) moving from time $t - 1$ to t and then to $t + 1$. The corresponding voltage gradient matrix can be calculated as follows:

$$\Delta V(t-1, t) = \begin{bmatrix} 0 & 0 & 0 & \Delta V_{14}^t(-) & \Delta V_{15}^t(-) & \Delta V_{16}^t(-) \\ \Delta V_{21}^t(+) & 0 & 0 & \Delta V_{24}^t(-) & \Delta V_{25}^t(-) & \Delta V_{26}^t(-) \\ \Delta V_{31}^t(+) & 0 & \Delta V_{33}^t(+) & \Delta V_{34}^t(+) & \Delta V_{35}^t(+) & 0 \\ \Delta V_{41}^t(-) & 0 & \Delta V_{43}^t(+) & \Delta V_{44}^t(+) & \Delta V_{45}^t(+) & 0 \\ 0 & 0 & 0 & 0 & 0 & 0 \\ 0 & 0 & 0 & 0 & 0 & 0 \end{bmatrix} \quad (13)$$

$$\Delta V(t, t+1) = \begin{bmatrix} 0 & 0 & 0 & 0 & 0 & 0 \\ \Delta V_{21}^{t+1}(-) & \Delta V_{22}^{t+1}(+) & 0 & 0 & 0 & 0 \\ \Delta V_{31}^{t+1}(-) & \Delta V_{32}^{t+1}(+) & \Delta V_{33}^{t+1}(-) & \Delta V_{34}^{t+1}(-) & \Delta V_{35}^{t+1}(-) & 0 \\ 0 & 0 & \Delta V_{43}^{t+1}(-) & \Delta V_{44}^{t+1}(-) & \Delta V_{45}^{t+1}(-) & 0 \\ 0 & 0 & \Delta V_{53}^{t+1}(+) & \Delta V_{54}^{t+1}(+) & \Delta V_{55}^{t+1}(+) & 0 \\ 0 & 0 & \Delta V_{63}^{t+1}(+) & \Delta V_{64}^{t+1}(+) & \Delta V_{65}^{t+1}(+) & 0 \end{bmatrix} \quad (14)$$

Here, motion vectors are determined based on the indicated signs, from negative to positive.

IV. IMPLEMENTATION AND EXPERIMENTAL RESULTS

A. System Implementation

Fig. 5 shows components of our proposed low-power SoftSense node. The microcontroller unit consists of 3 sub-units: a waveform generator, an analog-digital converter (ADC), and a BLE communication module (RN-42 BLE Chip) The waveform generator generates low-power square-wave signal at 200kHz and applies it to sensing coil. The dual-coil sensing configuration has sub-coils of two different size and shape. The inner coil is connected in serial with a capacitor and then linked to a waveform generator to generate a magnetic

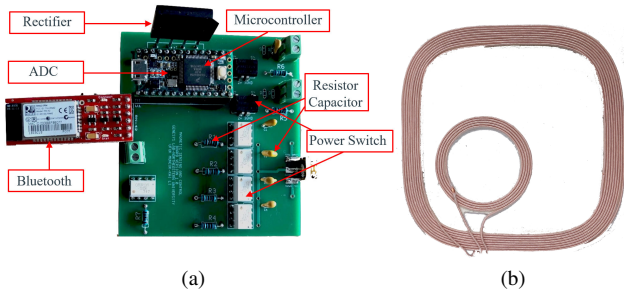


Fig. 5: SoftSense node (a) fabricated PCB board, and (b) fabricated dual-coil.

field by resonating at 200 kHz . The voltage rectifier converts the AC voltage at the outer coil into functional DC voltage. The presence of an object within the sensing coil coverage causes the voltage drop at the output of voltage rectifier. The analog digital converter in the microcontroller unit converts this voltage drop at the output of voltage rectifier into digital format. Fig. 5a shows the fabricated printed circuit board (PCB) of SoftSense prototype. We design the PCB board in two layers, one of which serves as a ground plane and fabricate it with FR-4 epoxy glass substrate. A Teensy 3.2 is used as microcontroller unit. It contains a 32 bit ARM Cortex-M4 72 MHz CPU and 12-bit analog digital converter. This unit performs functions of the waveform generator and analog digital converter. ON Semiconductor GBU8JFS-ND full-bridge rectifier chip is used as the voltage rectifier. Additionally, Fig. 5b shows our fabricated dual-coil made of litz wire with 1.15 mm diameter. This is same as the wire used in state-of-the-art Qi standard, with self-inductance of outer and inner coils being $20\ \mu\text{H}$ and $5\ \mu\text{H}$, respectively.

B. Experimental Results

In this section, we first evaluate the performance of our magnetic contactless sensing with other coil-based state-of-the-art techniques, and then study the ability to detect objects, identify their types, and track motion and direction of the movement. Fig. 6a compares power consumption between *inductive sensing* via a coil of the same size of the outer SoftSense coil connected to the wave generator, and *magnetic resonance sensing* consisting, again with the same coil size and a resonant capacitor connected to a wave generator. We set the sensing range up to 3cm for the purpose of comparison. Here the energy consumption includes microcontroller, circuit and coil energy consumption. Additionally, we compare them with Qi (i.e. WPC standard version 1.2) for two Qi configurations: (1) one sensing coil that results in 12% sensing area of a SoftSense node, and (ii) six overlapping coils that provide same sensing area as the SoftSense node. We observe that SoftSense consumes 18.5x less than the inductive sensing, 15x less than magnetic resonance sensing, 7.5x less than Qi with six coils, and 3.75x less than Qi with one coil. Fig. 6b compares sensing distance between Qi, inductive sensing, magnetic sensing, and SoftSense. Here, sensing distance is set as the maximum distance that a phone can be detected with %95 accuracy. Thus, SoftSense significantly outperforms

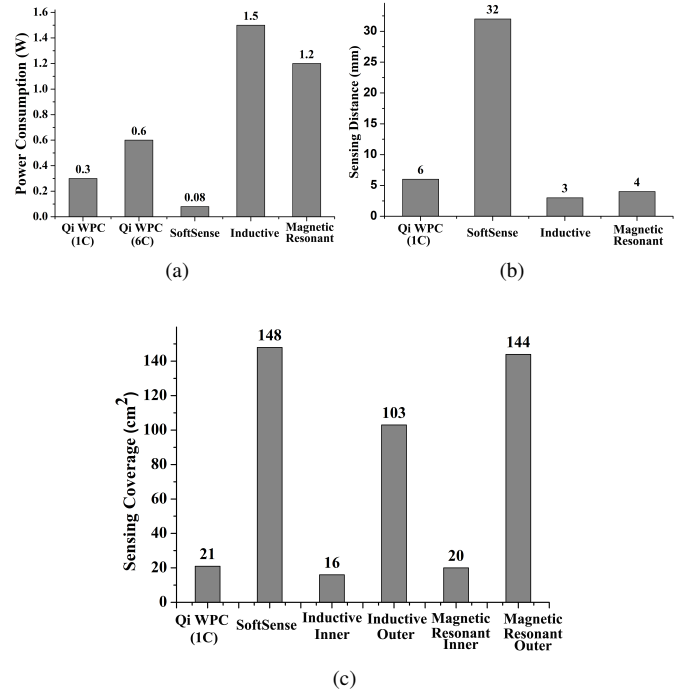


Fig. 6: Sensing performance comparison in terms of (a) power consumption, (b) sensing distance, and (c) sensing coverage.

other techniques with more than 5x margin. Fig. 6c depicts the sensing coverage and considers two sensing configurations for each of inductive and magnetic resonance sensing. We vary the coil dimensions to match the smaller inner SoftSense active coil, and also to match the size of the outer coil. We see that SoftSense provides the highest sensing coverage compared to other methods. Next, we evaluate the performance of SoftSense to identify the type of objects based on the measured voltage change. We train and test our classifier for seven objects with different sizes and shapes such as phone (iPhone X), laptop (Acer TravelMate X3), mouse (Logitech wireless mouse m275), metal plate (size $7\text{cm} \times 7\text{cm}$ and thickness of 1 mm), game controller (Xbox wireless controller), and power adapter (Belker 70w laptop charger). We conduct 150 experiments for each type of object, and for each experiment, we collect data with sampling rate 20ms for the duration of 5s. The nodes are placed on three over-surface materials: a large conference table with wood, a coffee shop table with hybrid wood, and a library table with hard plastic. The nodes are placed at distance 3cm from each other, ensuring the full sensing coverage of the surface.

Fig. 7a shows the average measured voltage changes for different object types when it is placed in the center of the coil. We see that regardless of surface materials, different objects introduce distinguishable variations in the voltage. In the following classification study, we conduct experiments for different overlapping areas between sensing coil and objects, as one of the SVM input features, along with the number of nodes that the object has covered. One of the main reason of misdetection error here is the hardware impairments due

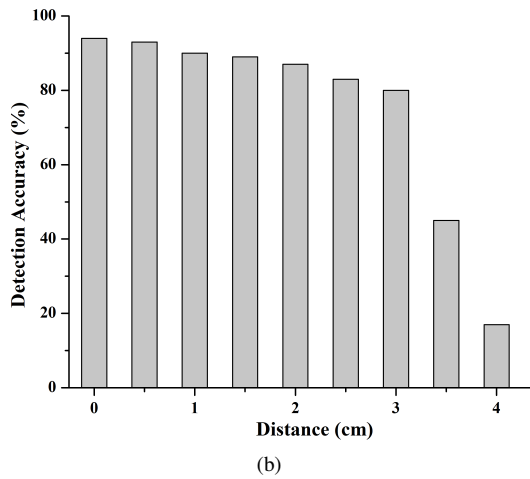
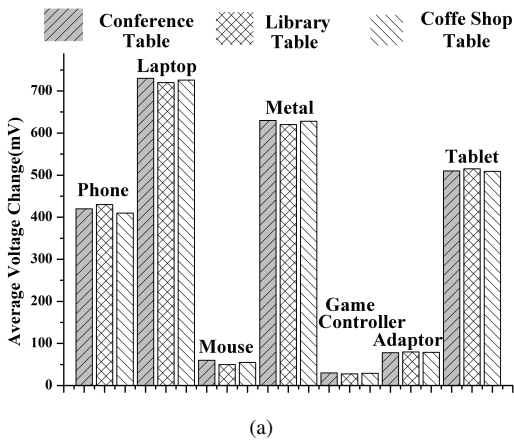


Fig. 7: (a) Average voltage change for different objects and three over-surface materials. Object detection accuracy for (b) different types of objects, and (c) different sensing distances.

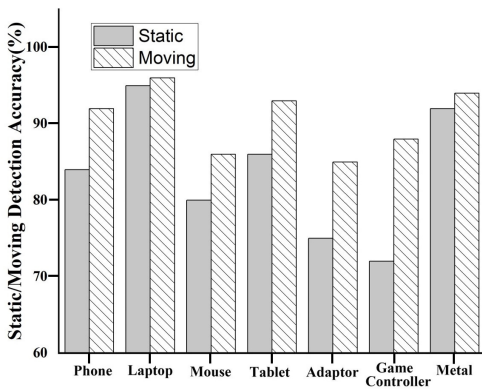


Fig. 8: Static and moving Object detection accuracy for different types of objects.

to ADC errors [11] such as analog-signal source resistance, analog-input signal noise, and ADC dynamic range change, on the sensing signal. Fig. 7b shows the results for detection accuracy at different sensing distances for the object type *phone*. It indicates 3 cm as the effective sensing distance here, which is similar for other object types. Finally, Fig. 8 presents the results for static object detection accuracy and

moving object detection accuracy for different types at the fixed sensing distance 3 cm. ADC errors that result in more than 100mV voltage change are enough to swap the signs of estimations in the voltage gradient from positive to negative or vice versa, which leads to misdetection. Despite such errors, Fig. 8 indicates the high accuracy of SoftSense object tracking. Furthermore, with multi-device sensing ability and high accuracy localization/tacking, we can easily apply the technique for phone and laptop surface charging, with only one phone and laptop power management separately. Overall, 8 of these nodes cover a $25\text{cm} \times 50\text{cm}$ surface, with a material cost of approximately 85 USD. Besides, by increasing the size of sensing coil to enhance the sensing distance, we can integrate this concept into car wireless charging.

V. CONCLUSION

This paper introduces a contactless magnetic sensing system with dual-coil configuration, with one coil as the driving loop, and the other is a passive coil that acts as a resonator relay. This configuration can extend the sensing distance to 3-4 cm using a 200 KHz AC signal source. The sensing system can robustly distinguish objects, such as a phone, laptop, metals, and mouse based on their voltage change with 94% accuracy and localize the position of the phone with cm accuracy. Our experiments on object tracking reveal 96% accuracy, with a total energy cost of 80 mW in each of these scenarios.

VI. ACKNOWLEDGEMENT

This work is supported by the funds available through the US National Science Foundation award CNS 1452628.

REFERENCES

- [1] M. Y. Naderi, K. R. Chowdhury, and S. Basagni, "Wireless sensor networks with rf energy harvesting: Energy models and analysis," in *2015 IEEE Wireless Communications and Networking Conference (WCNC)*. IEEE, 2015, pp. 1494–1499.
- [2] L. Chen, S. Cool, H. Ba, W. Heitzelmann, I. Demirkol, U. Muncuk, K. Chowdhury, and S. Basagni, "Range extension of passive wake-up radio systems through energy harvesting," in *2013 IEEE International Conference on Communications (ICC)*. IEEE, 2013, pp. 1549–1554.
- [3] D. Bharadia, K. R. Joshi, M. Kotaru, and S. Katti, "High throughput wifi backscatter," *ACM SIGCOMM Computer Comm. Review*, vol. 45, no. 4, pp. 283–296, 2015.
- [4] U. Ha, Y. Ma, Z. Zhong, T.-M. Hsu, and F. Adib, "Learning food quality and safety from wireless stickers," in *Proceedings of the 17th ACM Workshop on Hot Topics in Networks*. ACM, 2018, pp. 106–112.
- [5] W. P. Consortium. (2018) Qi-mobile computing. [Online]. Available: <https://www.wirelesspowerconsortium.com/qi/>
- [6] J. Sundeen and R. Buchanan, "Thermal sensor properties of cermet resistor films on silicon substrates," *Sensors and Actuators A: Physical*, vol. 90, no. 1-2, pp. 118–124, 2001.
- [7] Y. Zhang, G. Laput, and C. Harrison, "Electrick: Low-cost touch sensing using electric field tomography," in *CHI Conference on Human Factors in Computing Systems*. ACM, 2017, pp. 1–14.
- [8] L.-X. Chuo, Z. Luo, D. Sylvester, D. Blaauw, and H.-S. Kim, "RF-Echo: A non-line-of-sight indoor localization system using a low-power active rf reflector asic tag," in *Proceedings of Mobicom 2017*, 2017, pp. 222–234.
- [9] J. Jadidian and D. Katabi, "Magnetic mimo: How to charge your phone in your pocket," in *Proceedings of ACM Mobicom 2014*, 2014, pp. 495–506.
- [10] A. Kurs, A. Karalis, R. Moffatt, J. D. Joannopoulos, P. Fisher, and M. Soljačić, "Wireless power transfer via strongly coupled magnetic resonances," *Science*.
- [11] I. Freescale Semiconductor. (2016) Capacitor tolerance. [Online]. Available: <https://www.nxp.com/docs/en/application-note/AN5250.pdf>